Chapter 4

Effects of multi-slip and distinct heat source on MHD Carreau nanofluid flow past an elongating cylinder using statistical method *

4.1 Introduction

Viscous fluid flow over an expanding cylinder has important applications in industry and engineering fields. Production of plastic films, rubber, copper wires, and paper are some industrial applications of viscous fluid flows. The heat transfer rate and stretching determines the quality and finishing of a product. Slip flow plays a significant role in engineering and medical field. Micro valves, hard disk drives, internal cavities and nozzles are a few examples where the slip flow is utilized. Carreau nanofluid fluid flow over an elongating cylinder with multiple slip effects has been investigated in the chapter. ESHS and LHS effects are incorporated in the current study. Numerical solutions of the problem are obtained by transforming the system of PDEs into a system of ODEs and hence solving the transformed system using fourth order Runge Kutta coupled with shooting. The consequence of various parameters on heat transfer rate for pseudo-plastic and dilatant fluids are inspected using multiple linear regression Furthermore, the response of different parameters on drag coefficient and mass transfer is quantified using slope of linear regression via data points.

*Published in: Heat Transfer (Wiley), 2021; 50 (6) 5652-5673

4.2 Mathematical formulation

A steady, incompressible two-dimensional flow of an electrically conducting Carreau nanofluid over an elongating cylinder with radius $r = \mathbb{R}$ is considered. A uniform magnetic field (of strength B_0) is administered along the r direction. Let the cylinder be fixed at origin, O and stretched with a velocity $\frac{a_v x}{l}$ along the x direction (see Figure 4.1). Simultaneous effects of LHS and ESHS are considered. C_w and T_w are the constant values of concentration and temperature at the stretching cylinder whereas the ambient values are denoted by T_∞ and C_∞ with r tending to infinity. The governing equations take the form ((I. Khan, Malik, Hussain, Khan, et al., 2017)):

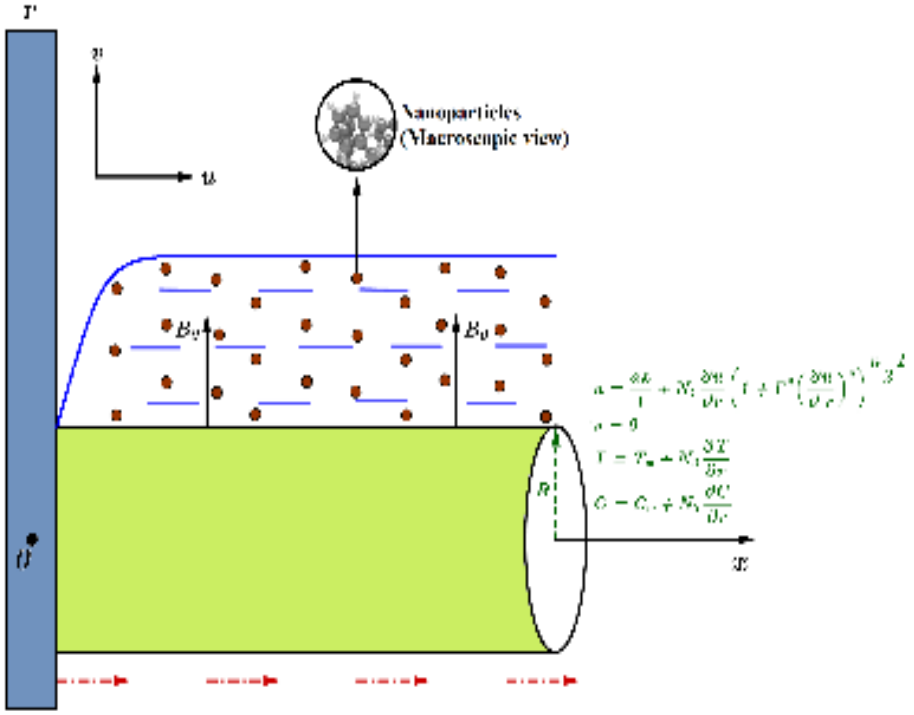

Figure 4.1: *Figurative representation*

$$\frac{\partial}{\partial x}(ru) + \frac{\partial}{\partial r}(rv) = 0 \tag{4.2.1}$$

$$u\frac{\partial u}{\partial x}+v\frac{\partial u}{\partial r}=\frac{\nu_f}{r}\frac{\partial u}{\partial r}\left(1+\Gamma^2\left(\frac{\partial u}{\partial r}\right)^2\right)^{\frac{n-1}{2}}+\nu_f\frac{\partial^2 u}{\partial r^2}\left(1+\Gamma^2\left(\frac{\partial u}{\partial r}\right)^2\right)^{\frac{n-1}{2}}$$
$$+\nu_f\left(n-1\right)\Gamma^2\left(\frac{\partial u}{\partial r}\right)^2\frac{\partial^2 u}{\partial r^2}\left(1+\Gamma^2\left(\frac{\partial u}{\partial r}\right)^2\right)^{\frac{n-3}{2}}-\frac{\sigma_f B_0^2 u}{\rho_f} \tag{4.2.2}$$

$$u\frac{\partial T}{\partial x}+v\frac{\partial T}{\partial r}=\alpha_f\left(\frac{\partial^2 T}{\partial r^2}+\frac{1}{r}\frac{\partial T}{\partial r}\right)+\frac{\left(\ \rho C_p\ \right)_p}{\left(\ \rho C_p\ \right)_f}\left(D_B\frac{\partial C}{\partial r}\ \frac{\partial T}{\partial r}+\frac{D_T}{T_\infty}\left(\frac{\partial T}{\partial r}\right)^2\right)$$
$$+\frac{q_T}{\left(\ \rho C_p\ \right)_f}\left(T-T_\infty\right)+\frac{q_E}{\left(\ \rho C_p\ \right)_f}\left(T_w-T_\infty\right)\ e^{\frac{-m\left(r^2-\mathbb{R}^2\right)}{2\mathbb{R}}\sqrt{\frac{a}{l\nu_f}}} \tag{4.2.3}$$

$$u\frac{\partial C}{\partial x}+v\frac{\partial C}{\partial r}=D_B\left(\frac{\partial^2 C}{\partial r^2}+\frac{1}{r}\frac{\partial C}{\partial r}\right)+\frac{D_T}{T_\infty}\left(\frac{\partial^2 T}{\partial r^2}+\frac{1}{r}\frac{\partial T}{\partial r}\right) \tag{4.2.4}$$

with

$$\left.\begin{array}{c} u=\frac{a_v x}{l}+N_1\frac{\partial u}{\partial r}\left(1+\Gamma^2\left(\frac{\partial u}{\partial r}\right)^2\right)^{\frac{n-1}{2}},\quad v=0,\\ T=T_w+N_2\frac{\partial T}{\partial r},\quad C=C_w+N_3\frac{\partial C}{\partial r}\quad when\ r=\mathbb{R}\\ u\to 0,\quad T\to T_\infty\ ,\quad C\to C_\infty\quad when\quad r\to\infty \end{array}\right\} \tag{4.2.5}$$

The following similarity variables ((Salahuddin et al., 2017)) are implemented in converting the above system of PDEs into a system of ODEs:

$$\left.\begin{array}{c} u=\frac{1}{r}\frac{\partial \psi}{\partial r},\quad v=\frac{-1}{r}\frac{\partial \psi}{\partial x},\quad \psi=\sqrt{\frac{a_v\nu_f}{l}}x\mathbb{R}f\left(\zeta\right),\\ \zeta=\left(\frac{r^2-\mathbb{R}^2}{2\mathbb{R}}\right)\sqrt{\frac{a_v}{l\nu_f}},\quad \theta=\frac{T-T_\infty}{T_w-T_\infty},\quad \phi=\frac{C-C_\infty}{C_w-C_\infty} \end{array}\right\} \tag{4.2.6}$$

The transformed equations are:

$$ff''+\left(n-1\right)We^2\kappa(f'')^3\left(1+We^2(f'')^2\right)^{\frac{n-3}{2}}+2\kappa f''\left(1+We^2(f'')^2\right)^{\frac{n-1}{2}}$$
$$-Mf'-\left(f'\right)^2+\left(1+2\kappa\zeta\right)f'''\left(1+We^2(f'')^2\right)^{\frac{n-1}{2}}$$
$$+\left(n-1\right)We^2\left(1+2\kappa\zeta\right)\left(f''\right)^2f'''\left(1+We^2(f'')^2\right)^{\frac{n-3}{2}}=0 \tag{4.2.7}$$

$$\left(1+2\kappa\zeta\right)\theta''+2\kappa\theta'+Pr\ f\ \theta'+\mathrm{Pr}\ \ \left(1+2\kappa\zeta\right)\left[Nb\phi'\theta'+Nt\ \left(\theta'\right)^2\right]+Pr\ Q_T\ \theta$$
$$+Pr\ Q_E\ e^{-m\zeta}=0 \tag{4.2.8}$$

$$\left(1+2\ \kappa\ \zeta\right)\ \phi''+\frac{Nt}{Nb}\ \left(1+2\ \kappa\ \zeta\right)\ \theta''+2\ \kappa\left[\phi'+\frac{Nt}{Nb}\ \theta'\right]+Sc\ f\ \phi'=0 \tag{4.2.9}$$

with

$$\left.\begin{array}{c} f\left(0\right)=0,\quad f'\left(0\right)=1+b_1f''\left(0\right)\left[1+We^2f''(0)^2\right]^{\frac{n-1}{2}},\quad \theta\left(0\right)=1+\gamma\theta'\left(0\right),\\ \phi\left(0\right)=1+b_3\phi'\left(0\right),\quad f'\left(\infty\right)\to 0,\quad \theta\left(\infty\right)\to 0,\quad \phi\left(\infty\right)\to 0 \end{array}\right\} \tag{4.2.10}$$

where the nondimensional parameters are taken as follows:

$$\left.\begin{array}{c} We^2 = \frac{\Gamma^2\ {a_v}^3\ x^2\ r^2}{\nu_f\ l^3\ \mathbb{R}^2},\quad \kappa = \frac{1}{\mathbb{R}}\sqrt{\frac{\nu_f\ l}{a_v}}\ ,\quad Sc = \frac{\nu_f}{D_B},\ M = \frac{\sigma_f\ B_0^2\ l}{a_v\ \rho_f},\quad Pr = \frac{\nu_f}{\alpha_f} \\ Nb = \frac{(\ \rho C_p\ )_p\ D_B\ (C_w - C_\infty)}{\nu_f\ (\ \rho C_p\ )_f},\ Nt = \frac{(\ \rho C_p\ )_p\ D_T\ (T_w - T_\infty)}{T_\infty\ \nu_f\ (\ \rho C_p\ )_f}, Q_T = \frac{q_T\ l}{a_v\ (\ \rho C_p\ )_f}, Q_E = \frac{q_E\ l}{a_v\ (\ \rho C_p\ )_f} \end{array}\right\} \tag{4.2.11}$$

Drag coefficient (Cf), mass transfer rate (Sh) and heat transfer rate (Nu) are defined as follows ((I. Khan et al., 2017)):

$$Cf = \frac{\tau_{rx}}{\frac{1}{2}\rho_f\left(\frac{a_v x}{l}\right)^2}\quad ,\quad Sh = \frac{x q_m}{D_B\left(C_w - C_\infty\right)}\quad ,\quad Nu = \frac{x q_w}{k_f\left(T_w - T_\infty\right)} \tag{4.2.12}$$

where

$$\tau_{rx} = \left(\mu_f\left(\frac{\partial u}{\partial r}\right)\left[1 + \Gamma^2\left(\frac{\partial u}{\partial r}\right)^2\right]^{\frac{n-1}{2}}\right)_{r\ =\ \mathbb{R}},\quad q_m = -D_B\left(\frac{\partial C}{\partial r}\right)_{r\ =\ \mathbb{R}}\ , \quad q_w = -k_f\left(\frac{\partial T}{\partial r}\right)_{r\ =\ \mathbb{R}} \tag{4.2.13}$$

The reduced physical quantities (using (4.2.6)) take the form:

$$\frac{Cf(Re_x)^{\frac{1}{2}}}{2} = f''(0)\left(1 + We^2(f''(0))^2\right)^{\frac{n-1}{2}},\quad Sh(Re_x)^{-\left(\frac{1}{2}\right)} = -\phi'(0)\ , \quad Nu(Re_x)^{-\left(\frac{1}{2}\right)} = -\theta'(0) \tag{4.2.14}$$

4.3 Numerical solution

Table 4.1: *Comparison of* $Nu(Re_x)^{\frac{-1}{2}}$ *with* $We = \kappa = M = Q_T = Q_E = Nt = b_1 = \gamma = b_3 = 0$ *and* $Nb \to 0$

Pr	$Nu(Re_x)^{-\frac{1}{2}}$	
	(W. Khan & Pop, 2010)	RK4
0.7	0.4539	0.453932
2	0.9113	0.911359
7	1.8954	1.895428
20	3.3539	3.354174

The highly nonlinear coupled ODE (4.2.7) to (4.2.9) with corresponding boundary conditions (4.2.10) are solved by engaging Runge-Kutta method of fourth order together with shooting technique with an accuracy of 10^{-6}. For the numerical computation we have restricted infinity to 15 and a step size of 0.1 is chosen. The

accuracy of the numerical method is guaranteed by performing a restrictive study with the already published results of (W. Khan & Pop, 2010) and an excellent agreement (discussed in Table 4.1) is noted. Additionally, the numerical values computed using Runge-Kutta of fourth order (RK4) is compared with BVP5C and RKF45 which are presented in Table 4.2 and four-digit accuracy is obtained. To accomplish this, we assume:

$$f = h_1, \quad f' = h_2, \quad f'' = h_3, \quad \theta = h_4, \quad \theta' = h_5, \quad \phi = h_6, \quad \phi' = h_7 \tag{4.3.1}$$

Accordingly, equation (4.2.7)-(4.2.10) takes the form:

$$\begin{gathered} h_1^{'} = h_2, \quad h_2^{'} = h_3, \\ h_3^{'} = \frac{-2\ \kappa\ h_3\left(1+We^2\ h_3^2\right)^{\frac{n-1}{2}} -(n-1)We^2\ \kappa\ h_3^3\left(1+We^2\ h_3^2\right)^{\frac{n-3}{2}} +M\ h_2+h_2^2-h_1h_3}{\left[(1+2\ \kappa\ \zeta)\left(1+We^2\ h_3^2\right)^{\frac{n-1}{2}} +(n-1)We^2(1+2\ \kappa\ \zeta)h_3^2\left(1+We^2\ h_3^2\right)^{\frac{n-3}{2}}\right]} \\ h_4^{'} = h_5, \\ h_5^{'} = \frac{-2\ \kappa\ h_5-Pr\ h_1\ h_5-\mathrm{Pr}\ (1+2\ \kappa\ \zeta)\left[Nb\ h_5\ h_7+Nt\ h_5^2\ \right]-Pr\ Q_T\ h_4-Pr\ Q_E\ e^{-m\zeta}}{1+2\ \kappa\ \zeta} \\ h_6^{'} = h_7,\ h_7^{'} = \frac{-\frac{Nt}{Nb}(1+2\ \kappa\ \zeta)\ h_5^{'}-2\ \kappa\left[h_7+\frac{Nt}{Nb}\ h_5\right]-Sc\ h_1\ h_7}{1+2\ \kappa\ \zeta} \end{gathered} \tag{4.3.2}$$

The following initial conditions are considered:

$$\begin{gathered} h_1(0) = 0, \quad h_2(0) = 1 + b_1\ s_1[1 + We^2\ {s_1}^2]^{\frac{n-1}{2}}, \quad h_3(0) = s_1 \\ h_4(0) = 1 + \gamma\ s_2, \quad h_5(0) = s_2, \quad h_6(0) = 1 + b_3\ s_3, \quad h_7(0) = s_3 \end{gathered} \tag{4.3.3}$$

where $s_1,\ s_2,\ s_3$ are unknowns and are found using Newton-Raphson method with a suitable initial guess.

4.4 Result and discussion

The impact of velocity slip (b_1), thermal slip (γ), concentration slip (b_3), Weissenberg number (We), linear heat source parameter (Q_T), thermophoresis parameter (Nt), Hartmann number (M), exponential heat source parameter (Q_E), curvature parameter (κ), Brownian motion parameter (Nb) on concentration $(\phi(\zeta))$, temperature $(\theta(\zeta))$ and velocity $\left(f'(\zeta)\right)$ profiles are carefully studied through Figures 4.2 - 4.13. The Schmidt number (Sc) and Prandtl number (Pr) are fixed at 1 and 3 respectively.

The discrepancy in $f'(\zeta)$ due to an increase in b_1 is depicted in Figure 4.2. Augmentation in b_1 shows a reduction in $f'(\zeta)$ for both dilatant and pseudo-plastic

Table 4.2: *Comparison of* $-\frac{1}{2}Cf(Re_x)^{\frac{1}{2}}$ *with* $M = Q_T = Q_E = Nt = b_1 = \gamma = b_3 = 0$ *and* $Nb \to 0$

n	We	κ	$-\frac{1}{2}Cf(Re_x)^{\frac{1}{2}}$		
			BVP5C	RKF45	RK4
0.5	1	0.2	0.989702	0.989709	0.989709
	1	0.4	1.03995	1.039965	1.039965
	1	0.6	1.088334	1.088361	1.088361
	2	0.2	0.867191	0.867198	0.867198
	2	0.4	0.901331	0.901343	0.901343
	2	0.6	0.934526	0.934545	0.934545
	3	0.2	0.777193	0.777201	0.777201
	3	0.4	0.80436	0.804374	0.804374
	3	0.6	0.830948	0.830972	0.830972
1.5	1	0.2	1.145708	1.145708	1.145708
	1	0.4	1.239624	1.239625	1.239625
	1	0.6	1.332933	1.332936	1.332936
	2	0.2	1.247964	1.247965	1.247965
	2	0.4	1.367059	1.367061	1.367061
	2	0.6	1.485123	1.485127	1.485127
	3	0.2	1.335538	1.335539	1.335539
	3	0.4	1.474373	1.474375	1.474375
	3	0.6	1.61158	1.611585	1.611585

fluids. Mounting values of b_1 causes a reduction in the movement of fluid particles and hence $f'(\zeta)$ decreases. Figure 4.3 delineates the decrease in $\theta(\zeta)$ with increasing γ values. Physically, augmenting thermal slip parameter minimises the sensitivity of the fluid flow within the boundary layer which diminishes the amount of heat produced and thus reduces the temperature. It is further noted that the thermal boundary layer thickness of pseudo-plastic fluid is greater than dilatant fluid.

Figure 4.4 depicts the variation of $f'(\zeta)$ due to the enhancement in M. An augmentation in M produces Lorentz force and hence a resistance force acts in the direction opposite to the fluid flow which retards the velocity of both fluids. An increase in We escalates the relaxation time of Carreau nanofluid and the fluid thickness grows which implies that the velocity profile of shear thinning fluid reduces whereas $f'(\zeta)$ enhances in the case of shear-thickening fluid (shown in Figure 4.5). Figure 4.6 depicts the effect of We on $\theta(\zeta)$. An opposite nature is observed on $\theta(\zeta)$ for shear thinning and thickening fluid. Variation in $\theta(\zeta)$ concerning κ is described in Figure 4.7. Physically, an increase in κ reduces the cylinder's radius

and surface area associated with the fluid which declines the heat transfer rates and hence $\theta(\zeta)$ rises. Figure 4.8 elucidates the consequence of Nb on $\theta(\zeta)$. An increase in Nb promotes the random motion of nanoparticles which enhances the temperature profile. Growing Nt values causes the hot fluid particles to move towards the cold region increasing $\theta(\zeta)$ (illustrated in Figure 4.9).

Figures 4.10 and 4.11 describe the variation of $\phi(\zeta)$ due to a rise in Nb and Nt, respectively. An increase in Nb reduces the concentration profile whereas an increase in Nt increases $\phi(\zeta)$. Figures 4.12 and 4.13 illustrate the variation in $\theta(\zeta)$ with increasing Q_T and Q_E values. Both parameters enhance $\theta(\zeta)$. It is also noted that temperature profile due to variation in Q_E has faster convergence than the temperature profile due to varying Q_T. The simultaneous impact of differing

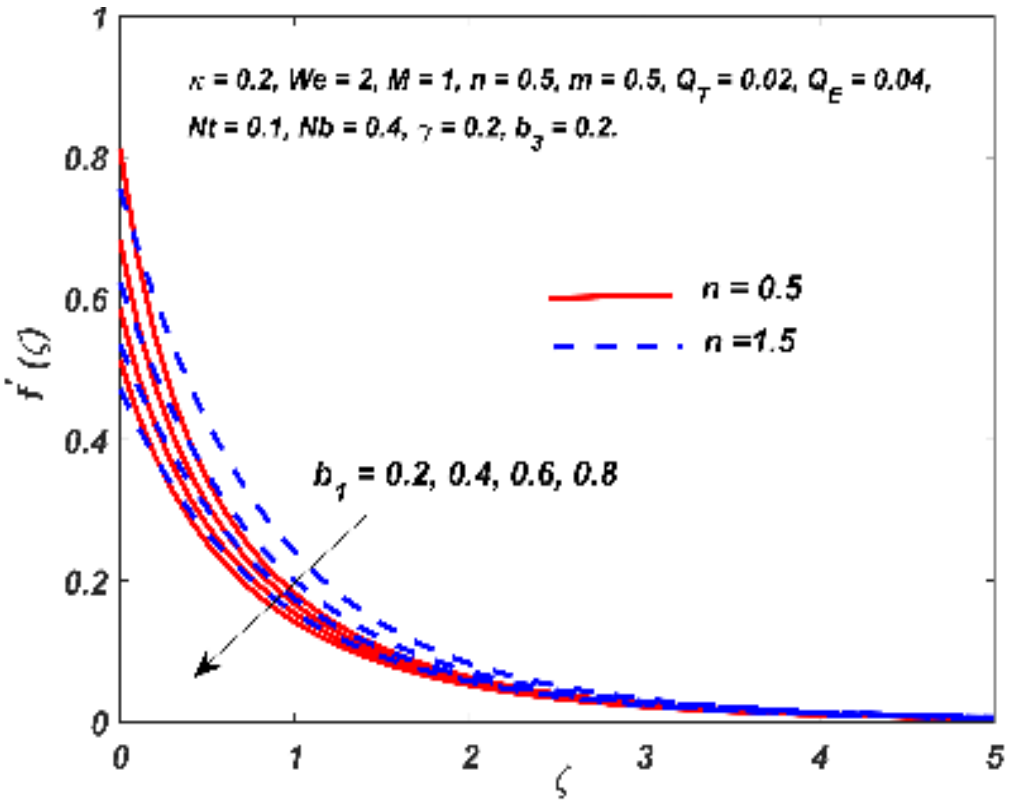

Figure 4.2: *$f'(\zeta)$ for differing b_1 values*

parameters on $Nu(Re_x)^{\frac{-1}{2}}$ is studied using surface plots which have been graphed in Figures $4.14 - 4.19$. The 4.14, 4.16, and 4.18 figures analyses the effects in case of shear thinning fluids while 4.15,4.17 and 4.19 figures examines the effects for

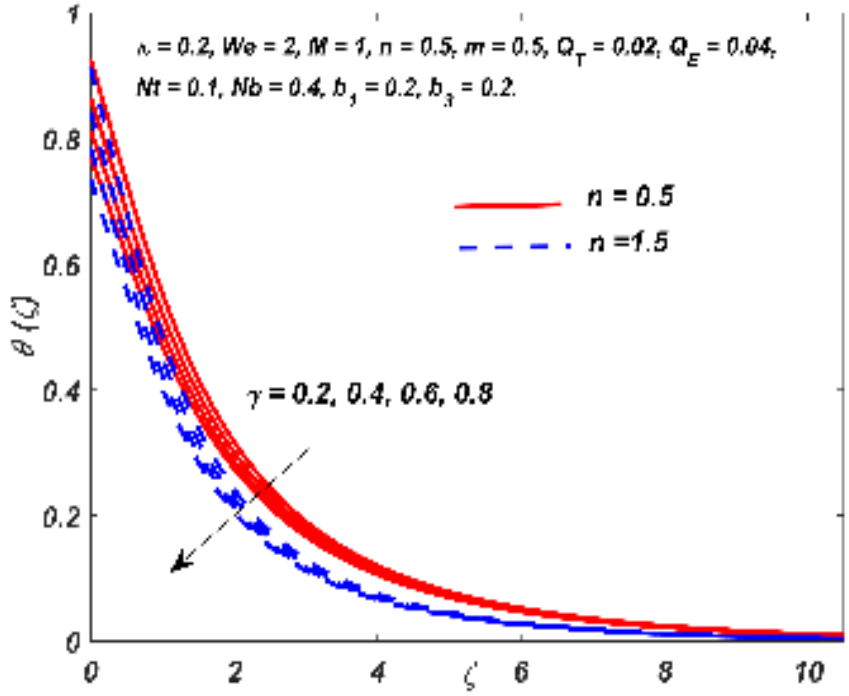

Figure 4.3: $\theta(\zeta)$ *for differing* γ *values*

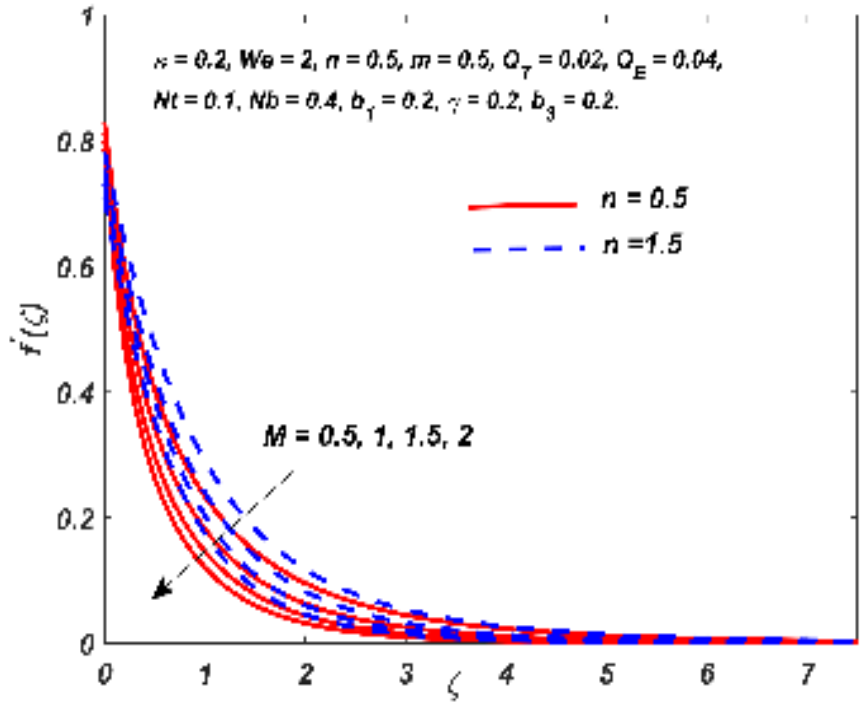

Figure 4.4: $f'(\zeta)$ *for differing* M *values*

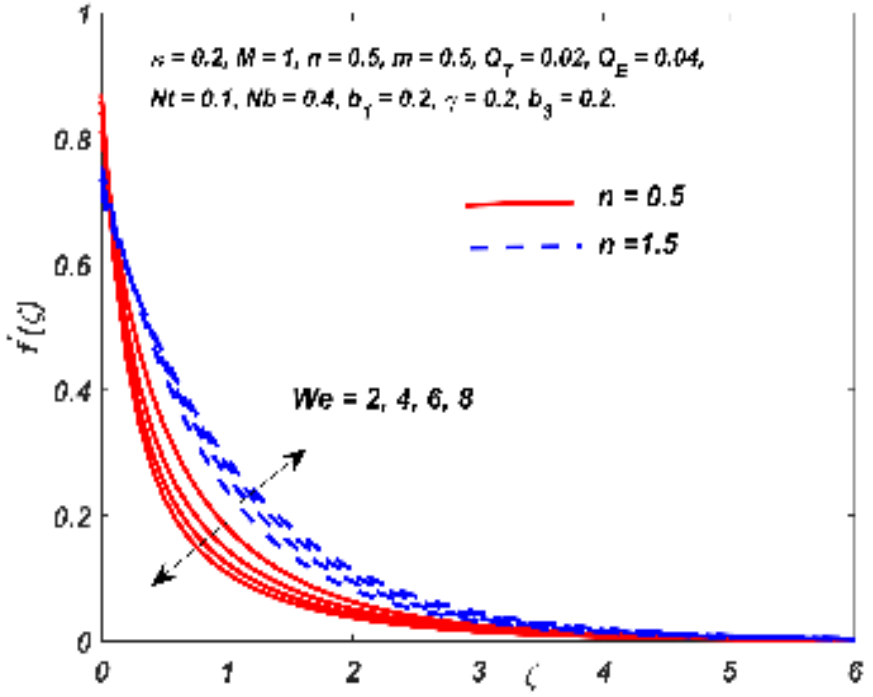

Figure 4.5: *$f'(\zeta)$ for differing We values*

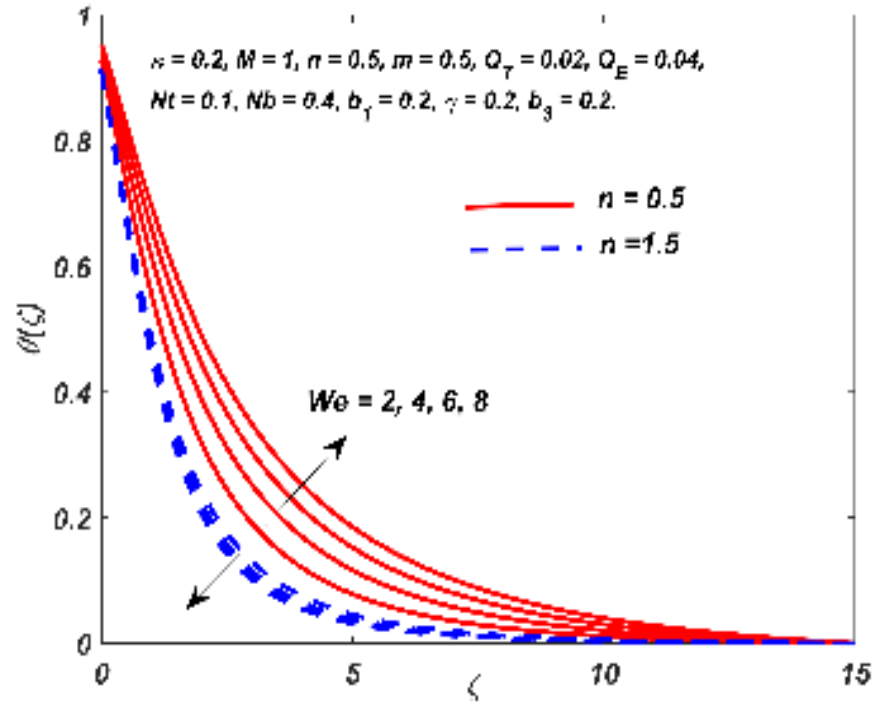

Figure 4.6: *$\theta(\zeta)$ for differing We values*

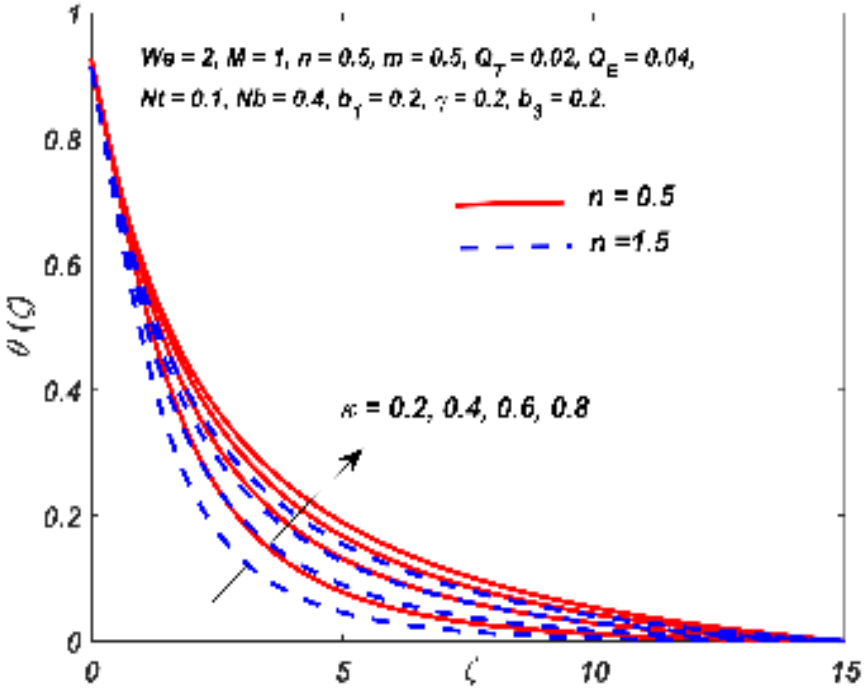

Figure 4.7: $\theta(\zeta)$ *for differing* κ *values*

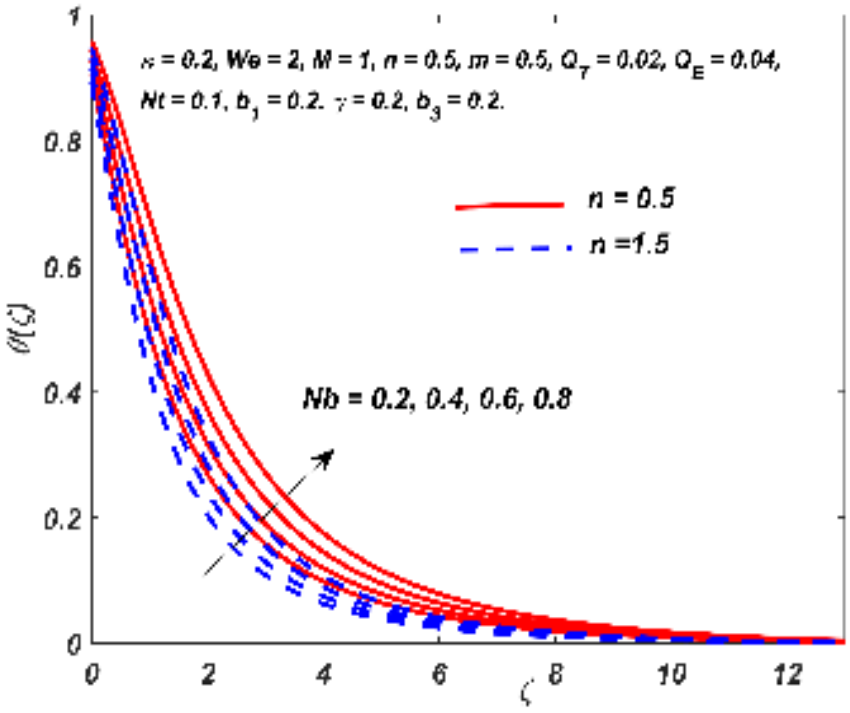

Figure 4.8: $\theta(\zeta)$ *for differing* Nb *values*

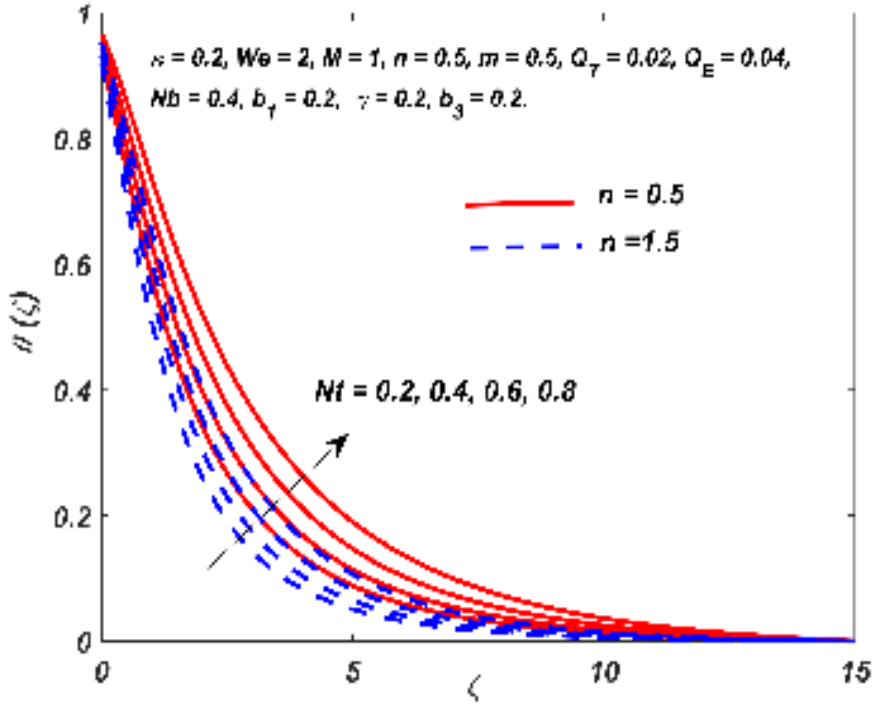

Figure 4.9: $\theta(\zeta)$ *for differing* Nt *values*

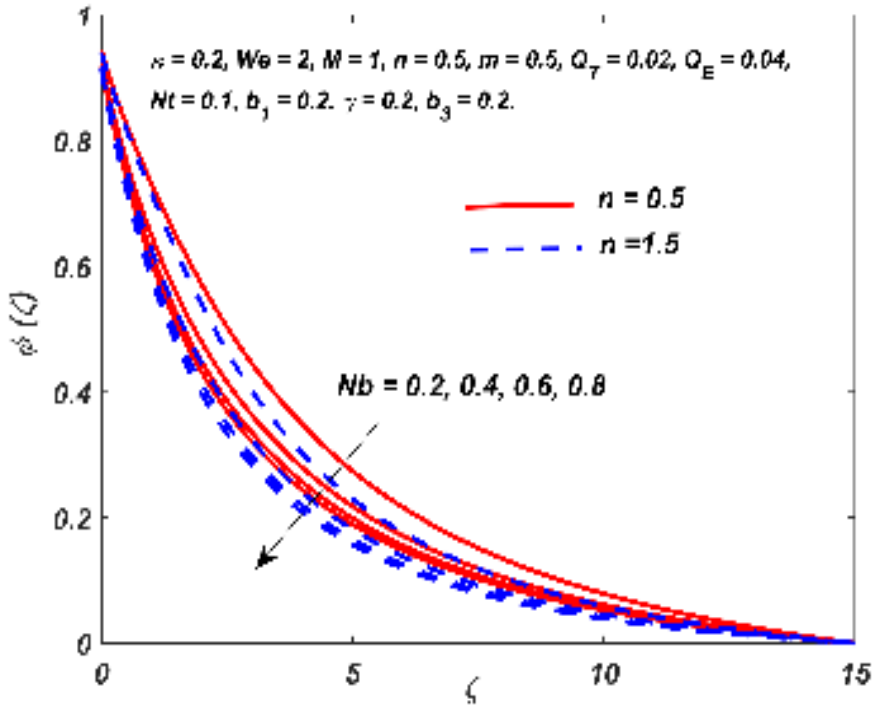

Figure 4.10: $\phi(\zeta)$ *for differing* Nb *values*

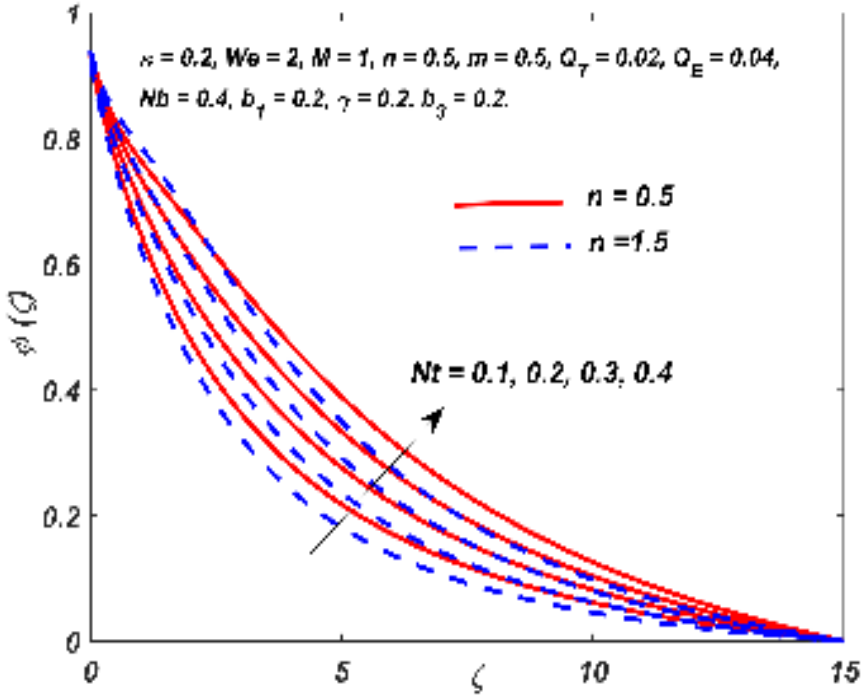

Figure 4.11: *$\phi(\zeta)$ for differing Nt values*

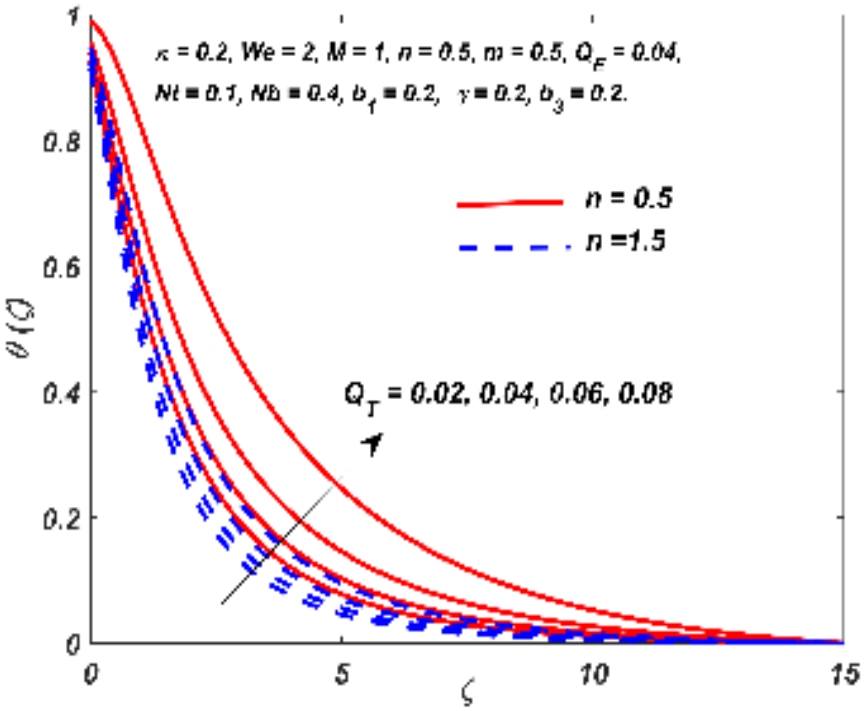

Figure 4.12: *$\theta(\zeta)$ for differing Q_T values*

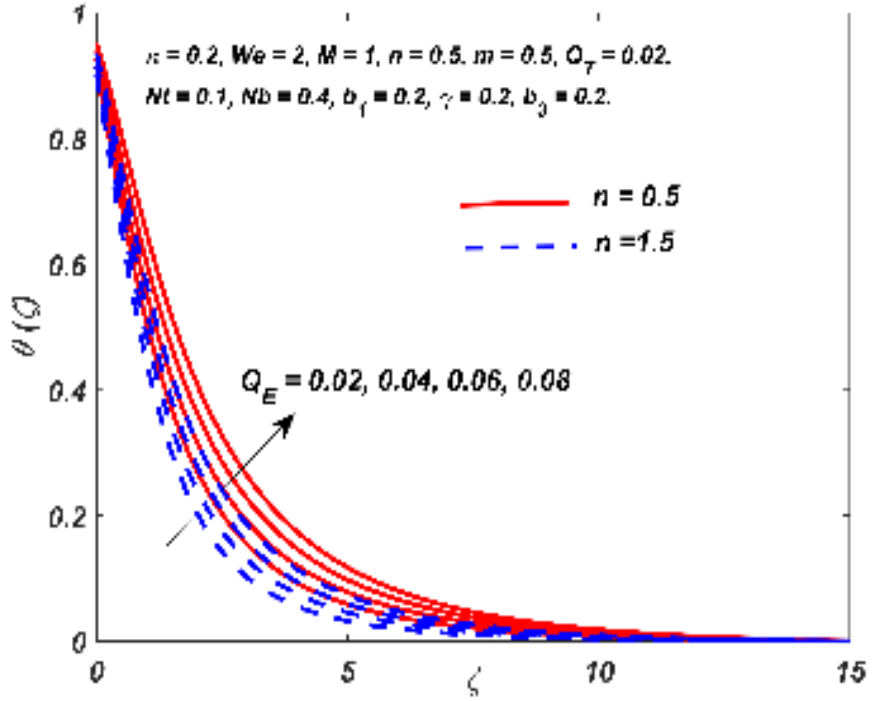

Figure 4.13: $\theta\,(\zeta)$ *for differing* Q_E *values*

shear thickening fluids. The impact of Nt and Nb on the heat transfer rate is described in Figures 4.14 and 4.15 with $\kappa = 0.2,\ We = 2,\ M = 1,\ m = 0.5,\ Q_E = 0.04,\ Q_T = 0.02$ and $b_1 = \gamma = b_3 = 0.2$. $Nu(Re_x)^{\frac{-1}{2}}$ diminishes for greater values of Nb and Nt in both cases ($n = 0.5$ and $n = 1.5$).

$Nu(Re_x)^{\frac{-1}{2}}$ is elevated with lower Q_T and Q_E values as shown in Figures 4.16 and 4.17 with $\kappa = 0.2,\ We = 2,\ M = 1,\ m = 0.5,\ Nb = 0.4,\ Nt = 0.1$ and $b_1 = \gamma = b_3 = 0.2$. The parallel effect of γ and κ on the heat transfer coefficient with $We = 2,\ M = 1, m = 0.5,\ Q_E = 0.04,\ Q_T = 0.02,\ Nb = 0.4,\ Nt = 0.1$ and $b_1 = b_3 = 0.2$ is explained in Figures 4.18 and 4.19. A rise in κ values enhances $Nu(Re_x)^{\frac{-1}{2}}$ whereas the heat transfer rate diminishes due to high thermal slip values. Hence, it can be concluded that $Nu(Re_x)^{\frac{-1}{2}}$ is directly proportional to κ and inversely proportional to Nt , Nb , Q_T , Q_E *and* γ. The consequence of different parameters on drag coefficient and Sherwood number when $n = 0.5$ and $n = 1.5$ is described in the table 4.3 and 4.4. Increment/decrement rate indicates the percentage change in the current value with respect to the previous value (preceding entry in the table). A positive sign denotes an increment while a negative sign indicates a decrement.

From table 4.3, it is understood that $-\frac{1}{2}Cf(Re_x)^{\frac{1}{2}}$ $\{for\ both\ cases\}$ increases with

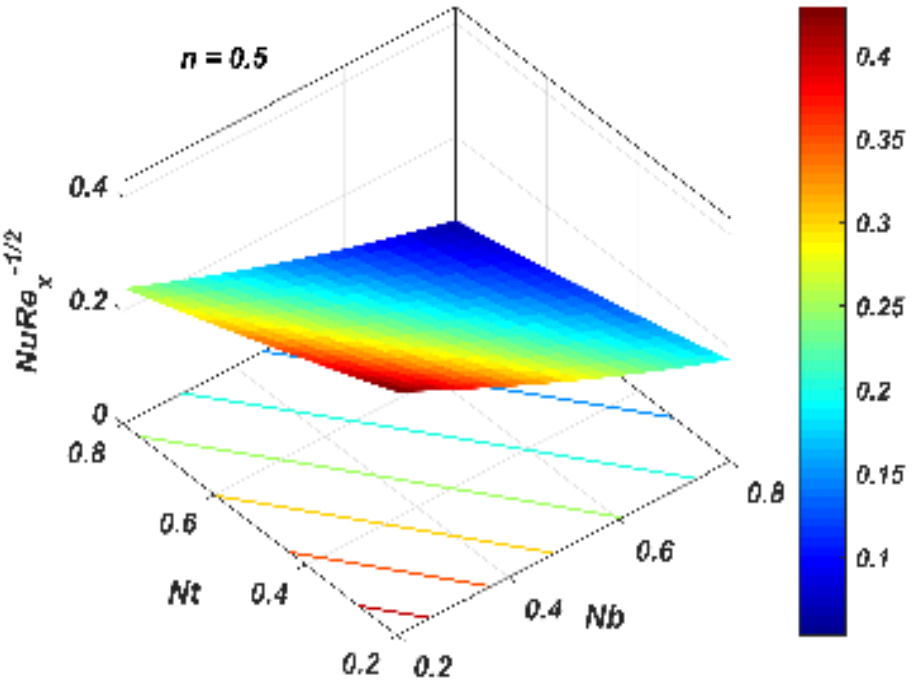

Figure 4.14: *Parallel effect of* Nb *and* Nt *on* $Nu(Re_x)^{\frac{-1}{2}}$ *when* $n = 0.5$

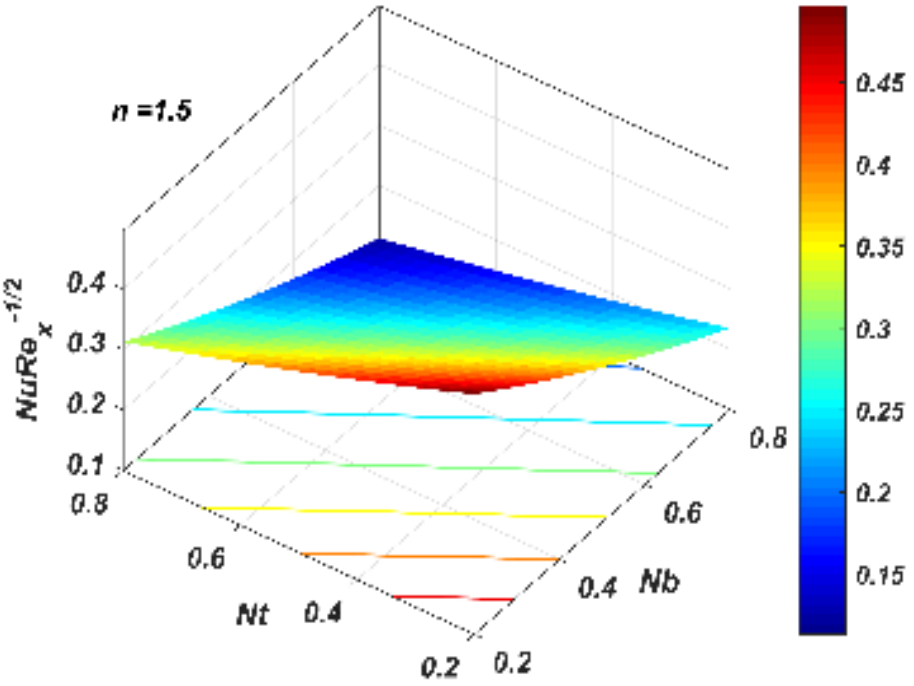

Figure 4.15: *Parallel effect of* Nb *and* Nt *on* $Nu(Re_x)^{\frac{-1}{2}}$ *when* $n = 1.5$

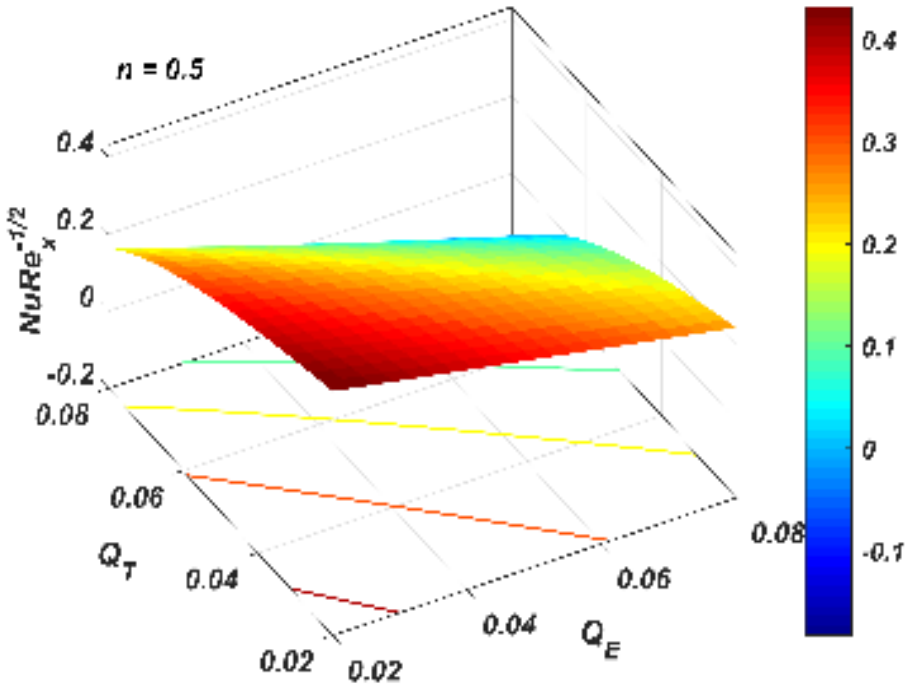

Figure 4.16: *Parallel effect of* Q_T *and* Q_E *on* $Nu(Re_x)^{\frac{-1}{2}}$ *when* $n = 0.5$

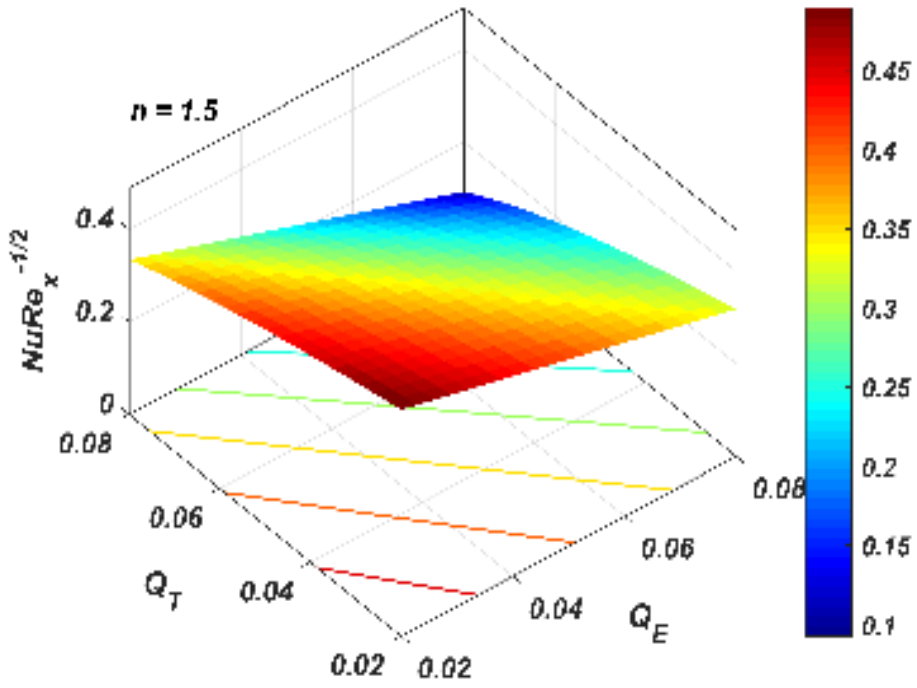

Figure 4.17: *Parallel effect of* Q_T *and* Q_E *on* $Nu(Re_x)^{\frac{-1}{2}}$ *when* $n = 1.5$

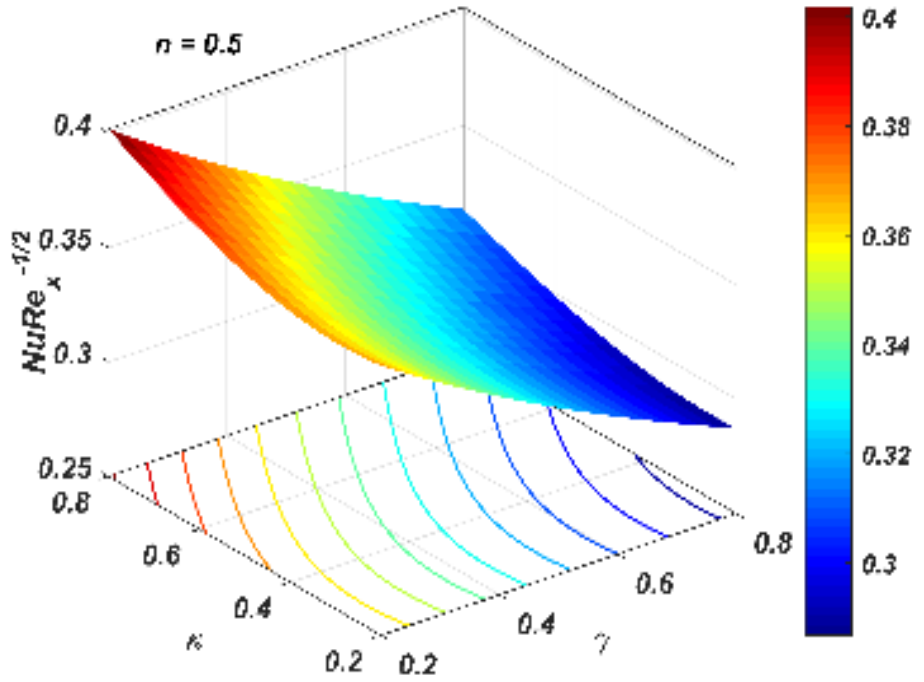

Figure 4.18: *Parallel effect of* γ *and* κ *on* $Nu(Re_x)^{\frac{-1}{2}}$ *when* $n = 0.5$

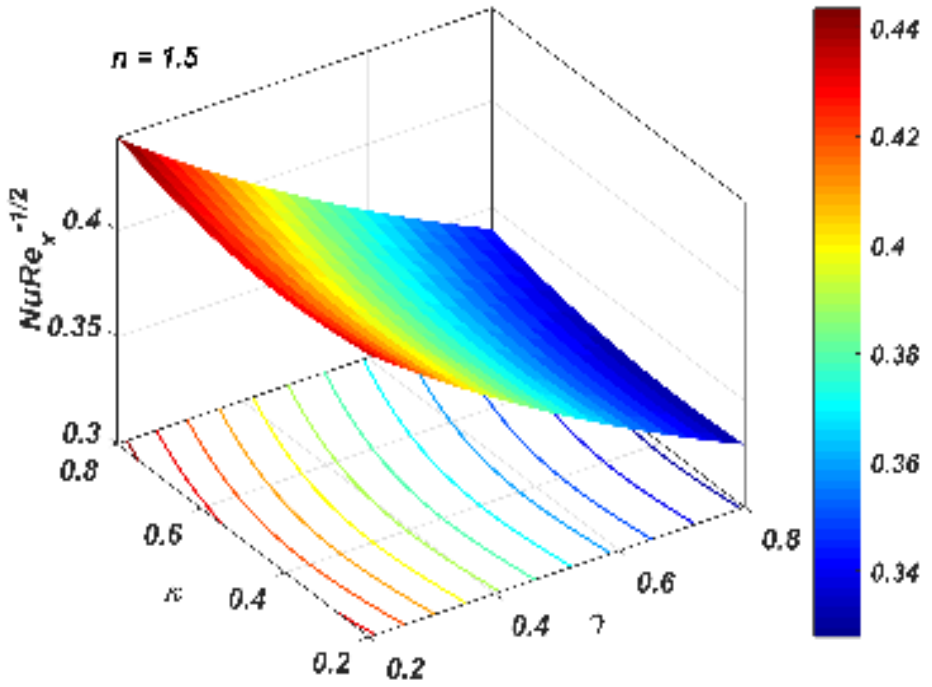

Figure 4.19: *Parallel effect of* γ *and* κ *on* $Nu(Re_x)^{\frac{-1}{2}}$ *when* $n = 1.5$

increase in κ and M values and decreases for increasing values of b_1. It is also seen that We has a negative response on $-\frac{1}{2}Cf(Re_x)^{\frac{1}{2}}$ $(when\ n = 0.5)$ and it is also seen that the result is reversed for $-\frac{1}{2}Cf(Re_x)^{\frac{1}{2}}$ $(when\ n = 1.5)$. From table 4.4, it is understood that κ and Nb enhances and Nt and b_3 diminishes the mass transfer rate.

The nature of variation in Sherwood number and skin friction coefficients due to different parameters has been quantified in table 4.3 and 4.4 using slope of linear regression. Positive slope implies that the corresponding parameter enhances the Sherwood number/drag coefficient. The magnitude of slope represents the rate of increase/decrease of drag coefficient/Sherwood number per unit value of the corresponding parameters.

Table 4.3: *Variation in* $-\frac{1}{2}Cf(Re_x)^{\frac{1}{2}}$ $\{at\ \zeta = 0\ \}$ *when* $\kappa = 0.2$, $We = 2$, $M = 1$, $m = 0.5$, $Q_T = 0.02$, $Q_E = 0.04$, $Nt = 0.1$, $Nb = 0.4$, $b_1 = 0.2$, $\gamma = 0.2$ *and* $b_3 = 0.2$

				$-\frac{1}{2}Cf(Re_x)^{\frac{1}{2}}$		**Increment(%)**	
We	κ	M	b_1	$n = 0.5$	$n = 1.5$	$n = 0.5$	$n = 1.5$
2				0.93454	1.225294		
4				0.789978	1.323258	-15.469	7.995
6				0.705486	1.391796	-10.695	5.18
8				0.648771	1.444318	-8.039	3.774
Slope				-0.04709	0.03628		
	0.2			0.93454	1.225294		
	0.4			0.960097	1.29569	2.735	5.745
	0.6			0.984375	1.361064	2.529	5.045
	0.8			1.007556	1.422289	2.355	4.498
Slope				0.121664	0.328178		
		0.5		0.845765	1.082917		
		1		0.93454	1.225294	10.496	13.148
		1.5		1.00619	1.342749	7.667	9.586
		2		1.066699	1.443231	6.014	7.483
Slope				0.146891	0.239679		
			0.2	0.93454	1.225294		
			0.4	0.795551	0.944656	-14.872	-22.904
			0.6	0.690287	0.775479	-13.232	-17.909
			0.8	0.608344	0.660741	-11.871	-14.796
Slope				-0.54193	-0.93142		

Table 4.4: *Variation in* $Sh(Re_x)^{-\frac{1}{2}}$ $\{at\ \zeta = 0\}$ *when* $\kappa = 0.2$, $We = 2$, $M = 1$, $m = 0.5$, $Q_T = 0.02$, $Nt = 0.1$ $Q_E = 0.04$, $Nb = 0.4$, $b_i = 0.2$, $\gamma = 0.2$ *and* $b_3 = 0.2$

				$Sh(Re_x)^{-\frac{1}{2}}$		Increment(%)	
κ	Nt	Nb	b_3	$n = 0.5$	$n = 1.5$	$n = 0.5$	$n = 1.5$
0.2				0.371478	0.396258		
0.4				0.459318	0.472917	23.646	19.346
0.6				0.541304	0.549809	17.849	16.259
0.8				0.616713	0.622549	13.931	13.23
Slope				0.408845	0.377883		
	0.1			0.371478	0.396258		
	0.2			0.339432	0.352109	-8.627	-11.142
	0.3			0.320597	0.320201	-5.549	-9.062
	0.4			0.314358	0.299672	-1.946	-6.411
Slope				-0.190197	-0.321665		
		0.2		0.28382	0.296854		
		0.4		0.371478	0.396258	30.885	33.486
		0.6		0.399384	0.428064	7.512	8.027
		0.8		0.412213	0.442835	3.212	3.451
Slope				0.206541	0.234875		
			0.2	0.371478	0.396258		
			0.4	0.340335	0.360624	-8.384	-8.993
			0.6	0.313986	0.330844	-7.742	-8.258
			0.8	0.291408	0.305591	-7.191	-7.633
Slope				-0.133281	-0.150891		

4.5 Statistical Analysis

4.5.1 Correlation and Probable Error

A statistical technique which helps in predicting the nature and quantity of relationship between two variables is known as correlation coefficient (r_c). The nature of relationship is elucidated using sign of r_c and its magnitude predicts the quantity of relationship. Nature of relationship is identified as positive or negative based on the relation. A positive value in r_c reflects that an increase in one variable correspondingly increases the other variable and a reverse nature is observed for a negative r_c value. Probable error (PE) guarantees the reliability of r_c and correlation is ought to be important ((Fisher et al., 1921)) when $\left|\frac{r_c}{PE}\right| > 6$; where $\tilde{n}$ denotes the number of observations and $PE = \left(\frac{1-{r_c}^2}{\sqrt{\tilde{n}}}\right) 0.6745$.

It is evident from table 4.5 that b_1, γ, M, Nb, Nt, Q_T and Q_E are negatively corre-

lated while κ exhibits a positive correlation with $Nu(Re_x)^{\frac{-1}{2}}$ $\{both\ cases\}$. It is also noted that We shows a differing nature on the heat transfer rate, i.e., r_c is positive in case of $Nu(Re_x)^{\frac{-1}{2}}$ $\{\text{n} = 1.5\}$ and negative for $Nu(Re_x)^{\frac{-1}{2}}$ $\{0.5\}$. From $\left|\frac{r_c}{PE}\right|$ values, it can be concluded that all the parameter of $Nu(Re_x)^{\frac{-1}{2}}$ $\{both\ cases\}$ are significant.

Table 4.5: *Probable error* (PE) *and correlation coefficient* (r_c) *of* $Nu(Re_x)^{\frac{-1}{2}}$

Parameter	$Nu(Re_x)^{\frac{-1}{2}}$ $(n = 0.5)$			$Nu(Re_x)^{\frac{-1}{2}}$ $(n = 1.5)$		
	r_c	PE	$\left\|\frac{r_c}{PE}\right\|$	r_c	PE	$\left\|\frac{r_c}{PE}\right\|$
Q_E	-1	0	2350568	-1	0	2572632.69
b_1	-0.99878	0.00073	1361.92	-0.99527	0.00284	349.98
γ	-0.99756	0.00147	678.85	-0.99705	0.00178	560.3
M	-0.99953	0.00028	3516.14	-0.99971	0.00017	5789.53
We	-0.99382	0.00372	267.47	0.96969	0.01801	53.85
κ	0.93349	0.03879	24.06	0.99667	0.002	497.15
Nb	-0.99886	0.00069	1453.69	-0.99903	0.00058	1712.46
Nt	-0.99948	0.00031	3183.46	-0.99918	0.0005	2012.09
Q_T	-0.97908	0.01249	78.41	-0.99531	0.00282	352.67

4.5.2 Regression Analysis

Multiple linear regression model of heat transfer rate (for n =0.5 and 1.5) is estimated using 45 set of values within the range $[0.2, 0.8]$ for b_1, γ, N_b, κ and Nt, $[0.02, 0.08]$ for Q_T and Q_E, $[0.5, 2]$ for M and $[2, 8]$ for We. The estimated model is given by:

$$Nu_{est}\,(n) = c + a_M\,M + a_{We}\,We + a_\kappa\,\kappa + a_{Nb}\,Nb + a_{Nt}\,Nt + a_{b_1}\,b_1 + a_\gamma\,\gamma + a_{Q_T}\,Q_T + a_{Q_E}\,Q_E \tag{4.5.1}$$

where c, a_{b_1}, a_γ, a_M, a_{We}, a_κ, a_{Nb}, a_{Nt}, a_{Q_T} and a_{Q_E} are the estimated regression coefficients. Nusselt number is estimated individually for $n = 0.5$ and $n = 1.5$ with the aid of MATLAB software. The estimated regression models are:

$$\begin{aligned} Nu_{est}\,(0.5) = {} & 1.03641 - 0.26072\,b_1 - 0.14210\,\gamma - 0.12386\,M - 0.02418\,We \\ & + 0.04218\,\kappa - 0.42863\,Nb - 0.29557\,Nt - 4.69465\,Q_T - 3.20600\,Q_E \end{aligned} \tag{4.5.2}$$

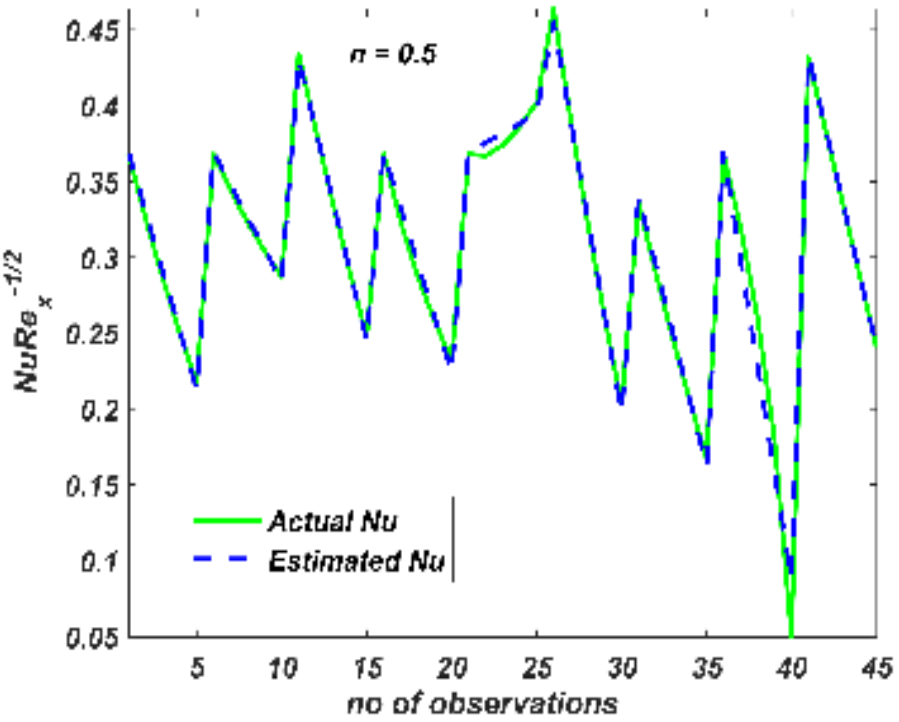

Figure 4.20: *Estimated versus actual* $Nu(Re_x)^{\frac{-1}{2}}$ *when* $n = 0.5$

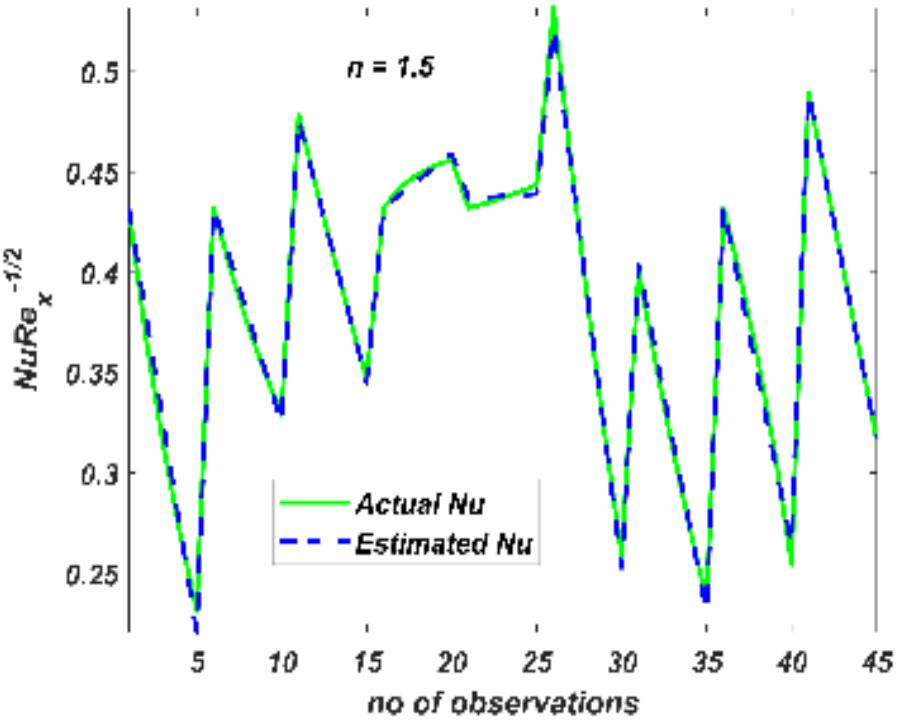

Figure 4.21: *Estimated versus actual* $Nu(Re_x)^{\frac{-1}{2}}$ *when* $n = 1.5$

$$Nu_{est}\,(1.5) = 0.99305 - 0.35222\ b_1 - 0.17913\ \gamma - 0.08699\ M + 0.00446\ We$$
$$+0.01121\kappa - 0.44799\ Nb - 0.28786\ Nt - 2.79750\ Q_T - 2.86966\ Q_E \tag{4.5.3}$$

The estimated regression coefficients are significant; since all p-values < 0.05. The accuracy of estimated regression models is described in Figure 4.20 and 4.21. It is understood that $b_1,\ \gamma,\ Nb,\ Nt,\ Q_T,\ Q_E$ and M have a negative response on the estimated $Nu\ \{both\ cases\}$. The estimated regression model predicts that the corresponding parameter induces a decreasing effect on Nu meaning that Nu decreases upon increasing parameter values. An increase in κ enhances the heat transfer coefficient $\{for\ both\ cases\}$. A reverse nature is observed due to increasing values of We for $n = 0.5\ and\ \ n = 1.5$. These results are in perfect synchronisation with the results discussed in table 4.5.

4.6 Conclusions

The key results of the current study are listed below:

- Hartmann number has a destructive effect on the velocity profile.
- Exponential space-based heat source (ESHS) and linear heat source (LHS) parameters exhibit a constructive behaviour on the temperature profile.
- Slip effect decreases the velocity and temperature profiles.
- Weissenberg number exhibits a differing nature on the velocity profile based on the nature of fluid; velocity is reduced when $n < 1$ and increased when $n > 1$.
- Velocity slip increases the drag coefficient whereas Hartmann number decreases the drag coefficient.
- Heat transfer rate lowers with ESHS, LHS and temperature slip parameters.
- Mass transfer rate is inversely proportional to concentration slip parameter.
- Nusselt number has been faultlessly estimated using multiple linear regression.